Antiproton, kaon, and muon capture by atomic hydrogen

Kazuhiro Sakimoto*
Institute of Space and Astronautical Science, Yoshinodai, Sagamihara 229-8510, Japan
(Received 24 April 2002; published 27 September 2002)

Capture of negatively charged, heavy particles by hydrogen atoms, i.e., $X^- + \mathrm{H} \rightarrow X^- p + e$, where $X^- = \bar{p}$ (antiproton), K^- (kaon), and μ^- (muon), is investigated by carrying out a rigorous full quantum-mechanical (QM) wave-packet calculation and a semiclassical (SC) calculation. An empirical law for the capture probabilities, found by the present author [Phys. Rev. A **65**, 012706 (2002)], is examined extensively by using the QM and SC results. The empirical law is useful to obtain reasonably accurate capture cross sections at center-of-mass translational energies less than 10 eV. Furthermore, a local-complex-potential (LCP) model is employed to discuss a quantum-mechanical effect of the relative motion at very low energies. The LCP calculation shows that a resonance structure is seen in the capture cross section.

DOI: 10.1103/PhysRevA.66.032506 PACS number(s): 36.10.−k, 34.50.Fa, 34.50.Lf

I. INTRODUCTION

Collision processes of hydrogen atoms with point charged particles, i.e., electrons, positrons, and protons, are of fundamental importance in atomic physics, and have been vigorously investigated both theoretically and experimentally. As an elementary subject, we should further consider the collisions with negatively charged, heavy particles (say X^-). As an example of X^-, we can choose antiprotons ($\bar{p}$), kaons (K^-), pions (π^-), or muons (μ^-), and these particles are much heavier than electrons. Recently, it has become possible to measure the atomic processes related to antiprotons or negative muons [1–5], and a further experimental progress in this field will be made in the near future [6,7]. Owing to the heavy mass and the negative charge, the collision processes of $X^- + \mathrm{H}$ have some interesting features clearly distinct from those of electron or proton impacts. Of particular importance is the adiabatic (Born-Oppenheimer) situation characterized by the presence of the so-called Fermi-Teller radius $R_{\mathrm{FT}} = 0.639$ a.u.; i.e., the electronically bound states become absent if the radial distance R between X^- and H is less than R_{FT}. We can easily understand that the electron emission occurs significantly in the $X^- + \mathrm{H}$ system even if the colliding particles slowly approach each other. When the center-of-mass (CM) translational energy E_{t} is less than the ionization threshold I ($= 13.6$ eV), the electron emission always leads to the capture of X^-, i.e.,

$$X^- + \mathrm{H}(1s) \rightarrow X^- p + e. \tag{1}$$

This reaction is also regarded as an important means of producing exotic atoms ($X^- p$), and the knowledge of a level distribution of the produced exotic atoms is essential in specifying the pathway to the decay by annihilation or nuclear absorption [8–15].

Since the capture process (1) is a three-body collision, it is strongly desired to solve the problem in a numerically accurate manner. However, we are confronted with two great difficulties in performing a rigorous full quantum-mechanical (QM) calculation for this process; (i) the electronic continuum states (i.e., electron emission) must be considered, and (ii) the particles X^- are captured into very high orbital states of $X^- p$. A close-coupling approach based on adiabatic-basis expansion, which is conventionally introduced for low-energy heavy particle collisions, is not an efficient numerical method for the electron emission, and a QM description of the collisions becomes troublesome when the highly excited states are related. Some approximations were introduced to perform QM calculations for the $\bar{p}$ capture [16] and the μ^- capture [17] although their applicability was severely limited. Very recently, the present author [18] has succeeded in carrying out a rigorous full QM calculation for the $\bar{p}$ capture. The time-dependent Schrödinger equation has been solved in a numerically direct manner; i.e, the time propagation of the wave packet has been performed on a gird of points in the configuration space. The direct solution is quite suitable to treat both the above mentioned problems (i) and (ii).

In Ref. [18], we have further found a useful empirical law for the $\bar{p}$ capture; i.e., the capture probability is deduced from merely the turning point of the $\bar{p} + \mathrm{H}$ relative radial motion irrespective of the translational energy. Once we know the relation between the capture probability and the turning point for some energy, we can easily estimate the probabilities or the cross sections for other energies. To explain the physical origin of the empirical law, the present author [19] has employed a time-dependent semiclassical (SC) theory and an adiabatic-basis expansion approach. In this SC picture, the relative motion is described classically, and the electron motion is described quantum mechanically. It has been further assumed that the adiabatic energy levels are degenerate in the transition region, and the rotational coupling is negligible. Then, we can obtain the following result for the transition-probability amplitude $a_{\Gamma\lambda}(t)$ with t being the time and (Γ,λ) specifying the adiabatic state:

$$\mathbf{a}(\infty) = \exp\left(-2 \int_{R_{\mathrm{tp}}}^{\infty} \mathbf{M} dR \right) \mathbf{a}(0), \tag{2}$$

where $\mathbf{a}(t) = \{a_{\Gamma\lambda}(t)\}$, R_{tp} is the turning point of the relative

*Email address: sakimoto@pub.isas.ac.jp

radial motion, and **M** is the radial coupling matrix. This approximation shows that the transition probability seen as a function of the turning point is independent of the translational energy and moreover of the X^- mass.

In the present paper, we study the capture process (1) for antiprotons, kaons, and muons, and examine to what extent the empirical law for the capture probabilities can be applied. We carry out rigorous QM calculations for energies $E_t = 5-10$ eV. Since the kaon and muon masses are, respectively, about $\frac{1}{2}$ and $\frac{1}{9}$ of the antiproton mass, these particles are useful to investigate the mass effect of the capture process (1). We argue on the mass independence as suggested from Eq. (2).

It is very interesting to study the capture process (1) at low energies. However, performing the time-dependent QM calculation at low energies $E_t \lesssim 1$ eV is not so easy because a very-long time propagation is required [18]. Hence, the empirical law will be very useful to study the capture at such low energies. In the present paper, we discuss the applicability of the empirical law for the low-energy capture. For this purpose, we use the results obtained by SC calculations. In the SC method, the numerical direct solution [20] is applied as in the time-dependent QM calculation. When $E_t > I$, it has been found [19] that the SC calculation gives reliable results of the probabilities for the electron emission if the relative radial motion is assumed to be a common trajectory determined by the adiabatic potential. We apply the SC method using the adiabatic potential to the capture process (1) that occurs at $E_t < I$. In the SC method, the relative motion is described classically. To discuss a QM effect of the relative motion at very low energies, we further introduce a local-complex-potential (LCP) model.

The present results are compared with those of previous studies using a classical trajectory Monte Carlo (CTMC) method [21–24] and using the SC method of Kwong *et al.* [25]. We also examine the adiabatic ionization (AI) [8,21,26] and Langevin [27] models. The $X^- + H$ system has a large capture probability close to unity when the distance of the collision pair becomes sufficiently small ($R \lesssim R_{FT}$). Therefore, the AI and Langevin models may be useful to estimate the capture cross section at very low energies.

II. THEORY

A. Quantum-mechanical theory

The total Hamiltonian is given by

$$\tilde{H} = -\frac{1}{2m_R}\frac{\partial^2}{\partial R^2}R + \frac{(\tilde{\mathbf{L}}-\tilde{\mathbf{l}})^2}{2m_R R^2} - \frac{1}{2m_r}\frac{\partial^2}{\partial r^2}r + \frac{\tilde{\mathbf{l}}^2}{2m_r r^2} + V(R,r,\theta), \tag{3}$$

where **R** and **r** denote the position vectors of X^--H and of e-p, respectively, m_R and m_r are the related reduced masses, $\tilde{\mathbf{L}}$ and $\tilde{\mathbf{l}}$ are the total and electronic angular momentum operators, respectively, V is the sum of all the Coulomb potentials, and θ is the angle between **R** and **r**. We employ a body-fixed (BF) frame in which the z axis is chosen along **R**, and the rotation from a space-fixed (SF) frame to the BF frame is represented by the Euler angles (α,β,γ). Atomic units are used unless otherwise stated. We solve the time-dependent Schrödinger equation

$$i\frac{\partial}{\partial t}\Psi^{LM(p)}(\mathbf{R},\mathbf{r},t) = \tilde{H}\Psi^{LM(p)}(\mathbf{R},\mathbf{r},t), \tag{4}$$

where L and M are the total angular momentum quantum number and its magnetic component in the SF frame, respectively, and $p = \pm$ is the total parity. The total wave function $\Psi^{LM(p)}$ can be expanded in the form

$$\Psi^{LM(p)}(\mathbf{R},\mathbf{r},t) = (Rr)^{-1}\sum_{\lambda} \bar{D}^{L(p)}_{M\lambda}(\alpha,\beta,\gamma)\psi^{L\lambda(p)}(R,r,\theta,t), \tag{5}$$

where $\lambda = \tilde{L}_z = \tilde{l}_z$, and

$$\bar{D}^{L(p)}_{M\lambda}(\alpha,\beta,\gamma) = \left[\frac{2L+1}{16\pi^2(1+\delta_{\lambda,0})}\right]^{1/2}[D^L_{M\lambda}(\alpha,\beta,\gamma) + p(-1)^{L+\lambda}D^L_{M-\lambda}(\alpha,\beta,\gamma)]^* \tag{6}$$

with $D^L_{M\lambda}(\alpha,\beta,\gamma)$ being the Wigner's rotation matrix element [28]. The initial condition of the total wave function (5) may be given from

$$\psi^{L\lambda(p)}(R,r,\theta,t=0) = \chi_0(r,\theta;R)\zeta(R)\delta_{\lambda 0}. \tag{7}$$

In the present study, the hydrogen atom is assumed to be initially in the $1s$ state, and hence the parity is given by $p = (-1)^L$. In Eq. (7), χ_0 is the ground-state adiabatic wave function of $X^- + H$ for fixed R, and $\zeta(R)$ is the Gaussian wave packet representing the incoming radial (R) motion. Since the range of translational energies $E_t < 10$ eV is considered, the transition to excited bound states of the hydrogen atom is energetically forbidden. Therefore, the capture probability can be calculated from [18]

$$P^L = 1 - \frac{1}{m_R|C(E)|^2}\mathrm{Im}[(F^L)^* G^L], \tag{8}$$

where

$$F^L(E) = \frac{1}{\sqrt{2\pi}}\int^{\infty} e^{iEt}\langle\chi_0|\psi^{L\lambda=0(p)}(t)\rangle_{R=R_0}dt, \tag{9a}$$

$$G^L(E) = \frac{1}{\sqrt{2\pi}}\int^{\infty} e^{iEt}\left\langle \chi_0\left|\frac{\mathrm{d}}{\mathrm{d}R}\psi^{L\lambda=0(p)}(t)\right.\right\rangle_{R=R_0} dt \tag{9b}$$

with $E = E_t - I$ being the total energy. The time integral in Eq. (9) is carried out at $R = R_0$ ($= 4$ a.u.) where the nonadiabatic coupling becomes negligible. The quantity $C(E)$ is the amplitude of the initial wave packet (7) with the total energy E [18].

The time propagation of $\psi^{L\lambda(p)}(R,r,\theta,t)$ with λ coupled is performed on a grid of points in the (R,r,θ) space by

using a discrete-variable-representation (DVR) technique described in Ref. [18]. The number of grid points used in the calculation is 60–300 for R, 20–40 for r, and 2 or 3 for θ. The states of $\lambda=0$ and 1 are coupled. These parameters have been chosen such that the capture probabilities are converged to within 1% in most cases and within 5% for high L where the capture probabilities are small. The central translational energy of the wave packet is chosen to be 7.5 eV, and the capture probabilities (8) are extracted for the energies $E_t=5-10$ eV.

B. Semiclassical theory

In the SC approximation, the variable R is treated in classical mechanics, i.e., $R=R(t)$, and the time-dependent Schrödinger equation becomes

$$i\frac{\partial}{\partial t}\Psi_{\rm SC}^{LM(p)}(\hat{\mathbf{R}},\mathbf{r},t)=\tilde{H}_{\rm SC}\Psi_{\rm SC}^{LM(p)}(\hat{\mathbf{R}},\mathbf{r},t), \tag{10}$$

where

$$\tilde{H}_{\rm SC}=\frac{(\tilde{\mathbf{L}}-\tilde{\mathbf{l}})^2}{2m_R R^2}-\frac{1}{2m_r r}\frac{\partial^2}{\partial r^2}r+\frac{\tilde{\mathbf{l}}^2}{2m_r r^2}+V(R,r,\theta). \tag{11}$$

The SC total wave function $\Psi_{\rm SC}^{LM(p)}(\hat{\mathbf{R}},\mathbf{r},t)$ can be written in the form similar to Eq. (5),

$$\Psi_{\rm SC}^{LM(p)}(\hat{\mathbf{R}},\mathbf{r},t)=r^{-1}\sum_{\lambda}\bar{D}_{M\lambda}^{L(p)}(\alpha,\beta,\gamma)\psi_{\rm SC}^{L\lambda(p)}(r,\theta,t). \tag{12}$$

The initial condition is simply given by

$$\psi_{\rm SC}^{L\lambda(p)}(r,\theta,t=0)=\chi_0(r,\theta;R_0)\delta_{\lambda 0}. \tag{13}$$

In the SC theory, we must provide the time dependence of the classical variable $R(t)$ since $\tilde{H}_{\rm SC}$ depends parametrically on R. We use the adiabatic potential to calculate the time dependence $R(t)$, that is,

$$E_t=\frac{m_R}{2}\left(\frac{dR}{dt}\right)^2+\frac{L(L+1)}{2m_R R^2}+V_{\rm ad}(R). \tag{14}$$

The adiabatic potential $V_{\rm ad}(R)$ is given by $V_{\rm ad}(R)=E_0(R)+I$, where $E_0(R)$ is the adiabatic energy of X^-+H. In this treatment, the relative radial distance R always diverges at $t\to\infty$, and the relative trajectories can never show any aspect of the capture. However, Refs. [18,19] have suggested that we can calculate the electron emission probability with reliable accuracy by using the trajectory obtained from Eq. (14). When $E_t<I$, the electron emission probability is just equal to the capture probability. Therefore,we may assume that the capture probability is given (at $E_t\leqslant 10$ eV) by

$$P_{\rm SC}^{L}=1-|\langle\chi_0(R_0)|\psi_{\rm SC}^{L\lambda=0(p)}(t_f)\rangle|^2, \tag{15}$$

where $t_f(>0)$ is defined by $R(t_f)=R_0$. The time-dependent equations for $\psi_{\rm SC}^{L\lambda(p)}(r,\theta,t)$ are solved using the same DVR method [20] as in the QM calculation. The number of grid points used in the calculation is 40 for r and 3 for θ. The states of $\lambda=0$ and 1 are coupled. These values are the largest ones chosen in the QM calculation.

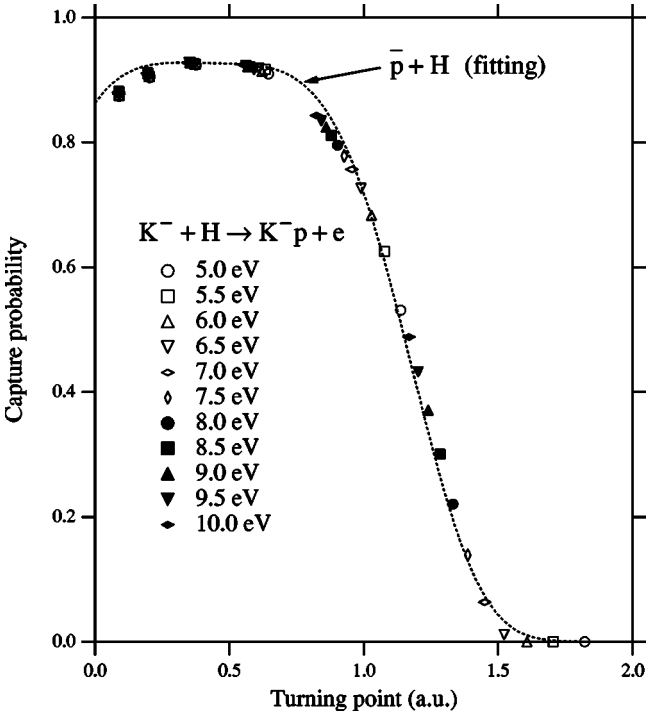

FIG. 1. K^-+H capture probabilities obtained by the QM calculation plotted against the turning point $R_{\rm tp}$ of the effective potential $V_{\rm eff}^L(R)$. The data points are for $L=10-35$ and $E_t=5-10$ eV. The broken line is the empirical fitting formula (17) for $\bar{p}+$H.

III. RESULTS AND DISCUSSION

A. Empirical law

In a previous QM study of $\bar{p}+$H [18], the capture probabilities for various L $(=0-54)$ and E_t $(=2.72-10$ eV) have been plotted against the turning point $R_{\rm tp}$ determined from the effective potential

$$V_{\rm eff}^L(R)=\frac{L(L+1)}{2m_R R^2}+V_{\rm ad}(R). \tag{16}$$

Then, it has been found that all the data points are put on a smooth line in a very good approximation. The fitting of all the data has been made in the form [18]

$$P_{\rm fit}^{\bar{p}}(R_{\rm tp})=\frac{88}{94.5+R_{\rm tp}}\exp[-2.3(R_{\rm tp}-0.426)^4]. \tag{17}$$

The approximation (2) suggests that the fitting formula (17) is further applicable irrespective of the X^- mass. To examine the mass dependence, we carry out the QM calculation for K^-+H. In Fig. 1, the K^- capture probabilities for various L $(=10-35)$ and E_t $(=5-10$ eV) are plotted together as a function of the turning point $R_{\rm tp}$. We can see that all the points almost lie on the curve (17). The ratio of the reduced

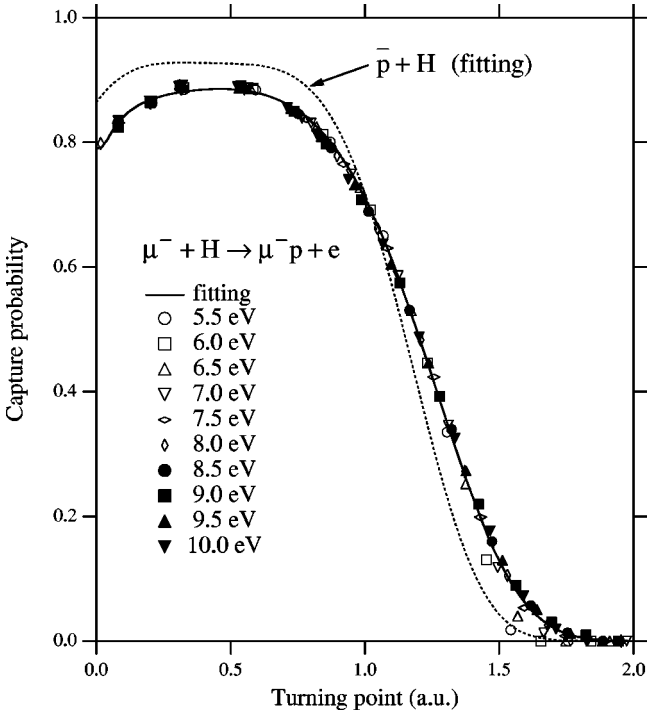

FIG. 2. μ^- + H capture probabilities obtained by the QM calculation plotted against the turning point R_{tp} of the effective potential $V^L_{eff}(R)$. The data points are for $L=2-24$ and $E_t=5.5-10$ eV. The solid line is the empirical fitting (18) for the μ^- + H data. The broken line is the empirical formula (17) for $\bar{p}$ + H.

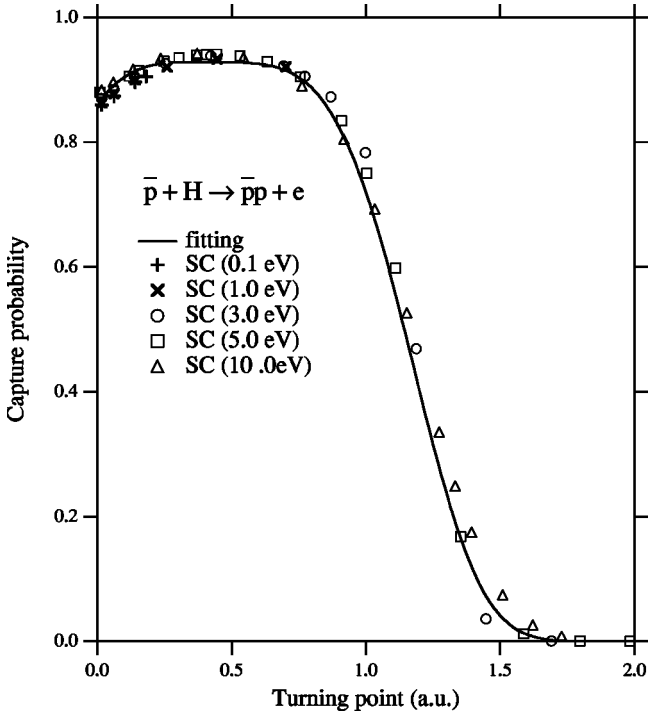

FIG. 3. $\bar{p}$ + H capture probabilities obtained by the SC calculation plotted against the turning point R_{tp} of the effective potential $V^L_{eff}(R)$. The data points are for $L=5-52$ and $E_t=0.1-10$ eV. The solid line is the empirical fitting formula (17) for $\bar{p}$ + H.

masses of K^- + H and $\bar{p}$ + H is about $\frac{2}{3}$. For the system having such mass difference, the fitting formula (17) is still applicable. We can easily estimate the probabilities for the K^- capture by using $P^{\bar{p}}_{fit}(R_{tp})$.

To examine the case that has a large mass difference, we carry out the QM calculation for μ^- + H. Figure 2 shows $P^{\bar{p}}_{fit}(R_{tp})$ and the μ^- capture probabilities for $L=2-24$ and $E_t=5.5-10$ eV. We find that the μ^- probabilities are smaller than $P^{\bar{p}}_{fit}(R_{tp})$ for $R_{tp}<1$ a.u., and are larger for $R_{tp}>1$ a.u. The ratio of the reduced masses of μ^- + H and $\bar{p}$ + H is about $\frac{1}{5}$. We see that this mass difference is so large that the mass independence cannot be assumed. However, as far as only the μ^- probabilities are concerned, the data are again well put on a curve. The fitting of the μ^- data gives

$$P^{\mu^-}_{fit}(R_{tp})=\left[0.79+0.12\exp\left(-\frac{0.0868}{R_{tp}}\right)\right]\exp(-0.236R^{5.2}_{tp}), \tag{18}$$

which is shown in Fig. 2. The deviation of the μ^- data from the fitting formula (18) is somewhat conspicuous for $R_{tp}\gtrsim 1.5$ a.u when the energy is low. The same result has been also found in the case of the $\bar{p}$ capture [18]. More details on the energy or mass dependence are discussed in Sec. III B.

Next, we consider the results obtained by the SC method using the adiabatic potential. Figure 3 shows the $\bar{p}$ + H capture probabilities for $L=5-52$ and $E_t=0.1-10$ eV as plotted against R_{tp}. Figure 4 shows the μ^- + H results for $L=2-25$ and $E_t=0.1-10$ eV. The SC results are compared with the fitting formula (17) or (18). We obtain reasonable agreements between the SC results and the fitting formula. Since the fitting formula is sufficiently reliable at high energies $E_t\geqslant 3$ or 5 eV, we can confirm the accuracy of the SC method using the adiabatic potential for the high energies. The deviation from the fitting formula is somewhat larger for the μ^- capture than for the $\bar{p}$ capture. This is probably because the QM effect of the relative motion is more important for the μ^- capture, as expected.

Figures 3 and 4 show that at the low energies $E_t\leqslant 1$ eV, the fitting formulas (17) and (18) well reproduce the SC probabilities. This suggests that the fitting formula and the SC method using the adiabatic potential are both reliable enough even at the low energies. Although the present QM calculation is not easily performed in the low-energy region, we can expect that the empirical formulas are useful to estimate the low-energy capture cross sections not only rapidly but also accurately. However, before drawing this conclusion, we should remember that the classical description is assumed for the relative motion in the SC method. The accuracy of this assumption for very low energies is examined in Secs. III D and III E.

B. Collision analysis by using the adiabatic potential

Previous SC studies [19,29] have shown that the relative motion of X^- + H can be practically described in terms of the adiabatic potential $V_{ad}(R)$ at least before the relative motion

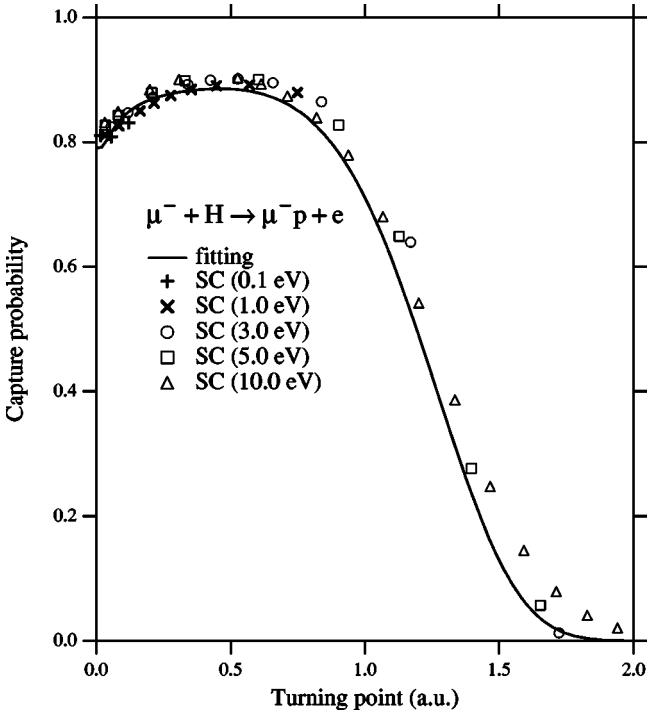

FIG. 4. $\mu^-+\mathrm{H}$ capture probabilities obtained by the SC calculation plotted against the turning point R_{tp} of the effective potential $V_{\mathrm{eff}}^L(R)$. The data points are for $L=2$–25 and $E_{\mathrm{t}}=0.1$–10 eV. The solid line is the empirical fitting formula (18) for $\mu^-+\mathrm{H}$.

takes the turning point. Therefore, the adiabatic potential will be very helpful in getting some knowledge of the $X^-+\mathrm{H}$ collision. Here, we discuss the energy or mass dependence of the capture process by using the adiabatic potential.

The adiabatic potential for $R>3$ a.u. can be well approximated by the polarization potential $-\alpha/2R^4$ [29], where α is the polarizability of the hydrogen atom. As seen later, the Langevin value $\sigma_{\mathrm{L}}=\pi(2\alpha/E_{\mathrm{t}})^{1/2}$ [27] gives a rough estimate of the cross section for the capture process (1) at very low energies. When $R<R_{\mathrm{FT}}$, the adiabatic potential is just equal to $V_{\mathrm{ad}}(R)=-R^{-1}+I$. (Although R is not the distance between X^- and p to be exact, the difference is negligible.) In this case, the turning point is given by $R_{\mathrm{tp}}=\{1-[1-2L(L+1)(I-E_{\mathrm{t}})/m_R]^{1/2}\}/[2(I-E_{\mathrm{t}})]$. The turning points for various energies and angular momenta are shown in Fig. 5. If L is such that $L(L+1)\ll m_R$, we have $R_{\mathrm{tp}}=L(L+1)/(2m_R)$, which is independent of the energy. This can be confirmed in Fig. 5 for $R_{\mathrm{tp}}\lesssim 0.25$ a.u. When R_{tp} is large, the turning point becomes strongly dependent on the energy. We further see from Fig. 5 that only the collisions with small turning points can contribute to the capture as the energy decreases. This is resulting from the orbiting phenomena.

It can be naturally understood that the mechanism of the electron emission becomes different whether R is larger or smaller than some critical distance such as R_{FT}. Once the relative distance becomes $R\lesssim R_{\mathrm{FT}}$, the electron has always a great chance to run away easily from the proton. The electron emission probability will be larger as the collision pair stays there longer. Therefore, a period of the stay in the region $R<R_{\mathrm{FT}}$ would be an important quantity to characterize the capture process. We consider the time T_{p} required for the passage from $R=R_{\mathrm{FT}}$ to R_{tp}. In Fig. 6, we show the passage time T_{p} calculated using the adiabatic potential for three energies of $E_{\mathrm{t}}=0.1$, 1, and 10 eV as a function of the turning point. We can see that the passage time becomes almost the same when the energy is low. This is because the effective potential $V_{\mathrm{eff}}^L(R)$ has a very deep well for low L. (When the

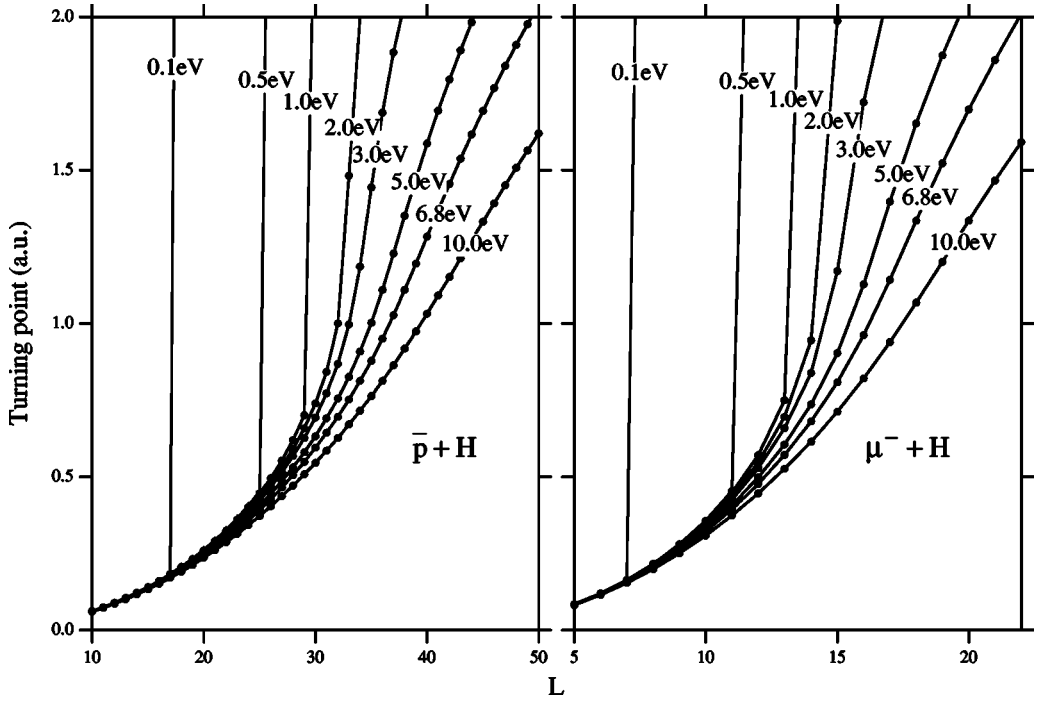

FIG. 5. Turning points R_{tp} of the effective potential $V_{\mathrm{eff}}^L(R)$ for $\bar{p}+\mathrm{H}$ and $\mu^-+\mathrm{H}$ as plotted against the angular momentum L.

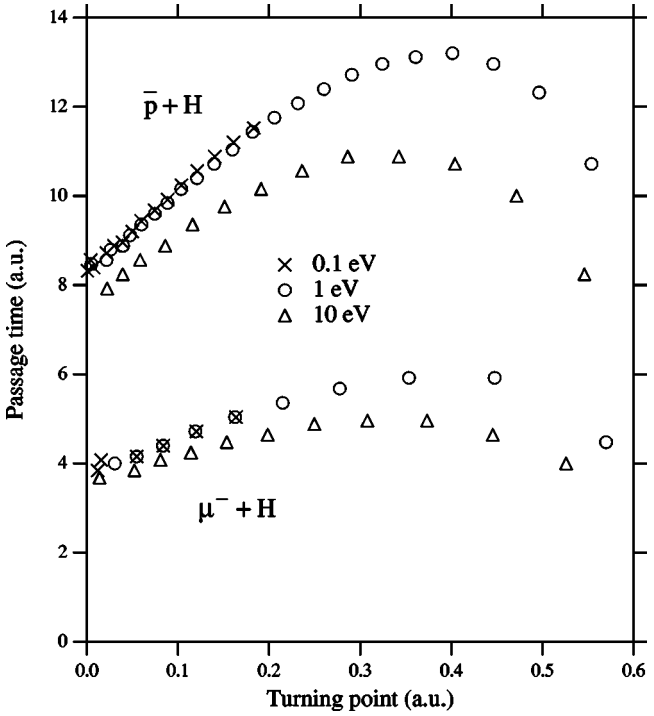

FIG. 6. Time T_p required for the passage from $R=R_{FT}$ to R_{tp} for $\bar{p}+H$ and μ^-+H at $E_t=0.1$, 1, and 10 eV as a function of the turning point R_{tp}.

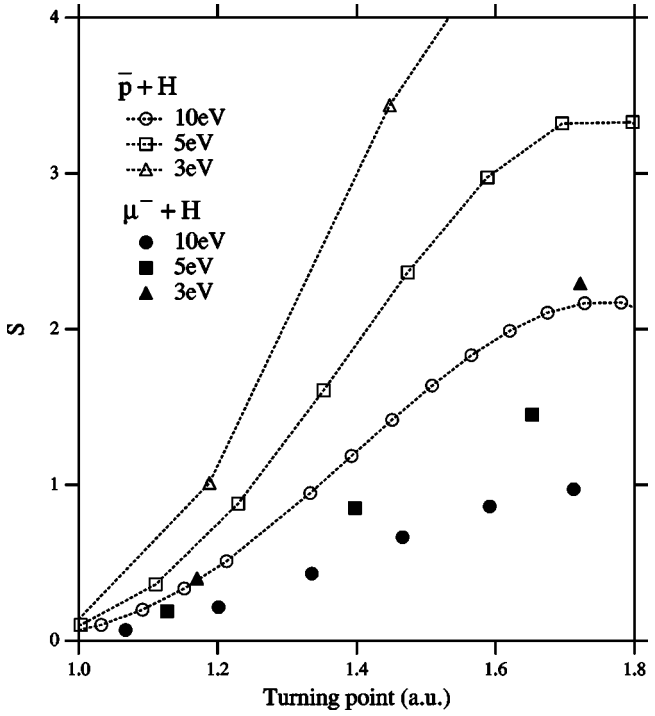

FIG. 7. Dimensionless quantities $S=\Delta E T_c$ defined by Eq. (19) for $\bar{p}+H$ and μ^-+H at $E_t=3$, 5, and 10 eV as a function of the turning point R_{tp}.

minimum position R_{min} is smaller than R_{FT}, the minimum value is $-m_R/[2L(L+1)]+I$.) However, the passage times for $\bar{p}+H$ and μ^-+H are clearly distinguished from each other. Since the passage time is directly proportional to $\sqrt{m_R}$, the ratio of the two passage times is always about $\sqrt{5}$. Consequently, we can understand that the μ^- capture probabilities are smaller than the $\bar{p}$ ones for small R_{tp}, as seen in Fig. 2. It should be noted that the K^- capture probabilities are slightly smaller than the $\bar{p}$ ones for $R_{tp}\lesssim 0.2$ a.u. (Fig. 1).

When $R_{tp}>R_{FT}$, the electron emission should be regarded as a nonadiabatic process. To characterize the adiabaticity of the collision, we introduce the dimensionless quantity

$$S=\Delta E T_c. \tag{19}$$

Here, since the turning point is the most important in the electron emission [18,29], the energy difference ΔE is chosen to be the AI energy at $R=R_{tp}$. From Figs. 1–4, we see that the capture occurs at $R\lesssim 2$ a.u. Therefore, we define the collision time T_c by the time required for the motion from $R=2$ a.u. to the turning point R_{tp}. We may expect that the collision process becomes more adiabatic as S increases. Figure 7 shows the values of S for $\bar{p}+H$ and μ^-+H. We see that the $\bar{p}$ collisions are generally more adiabatic than the μ^- collisions. When the collision becomes adiabatic, the capture occurs less frequently in distant encounters ($R>R_{FT}$). This would be the origin of the difference (seen in Fig. 2) between the fitting formulas (17) and (18) at $R_{tp}>1$ a.u.

When $R_{tp}\gtrsim 1.5$ a.u., Fig. 2 shows that the low-energy data for μ^-+H are much smaller than $P_{fit}^{\mu^-}(R_{tp})$, and rather close to $P_{fit}^{\bar{p}}(R_{tp})$. This may be explained again in terms of the adiabaticity parameter S. Figure 7 shows that the collisions of $\bar{p}+H$ at the high energy ($E_T=10$ eV) and of μ^-+H at the low energy ($E_t=3$ eV) have almost the same value of S. Differently from the case of $R_{tp}\lesssim R_{FT}$, we cannot always distinguish between the collision natures of $\bar{p}+H$ and μ^-+H for large R_{tp}. Anyway, the fitting formula (18) for $R_{tp}\gtrsim 1.5$ a.u. would not be so accurate at low energies. In regard to the calculation of the capture cross section, nevertheless, the fitting formula will be still useful even at low energies because the contribution of the large turning points to the cross section is less important with decreasing energy (Fig. 5).

C. Capture cross section

In the present study, the capture cross sections are calculated by the QM and SC methods and by using the fitting formulas (17) and (18). The fitting formulas are further used to estimate the cross sections at low energies down to 0.01 eV. To obtain the turning points in Eqs. (17) and (18), the centrifugal potential $L(L+1)/(2m_R R^2)$ is replaced by the classical one $E_t b^2/R^2$, with b being the (continuous) impact parameter. The use of $L(L+1)/(2m_R R^2)$ produces a saw-toothed structure in the energy dependence of the calculated cross sections. In reality, the cross section should have a smooth energy dependence because of the effect of tunneling or above-barrier reflection. Although the correction of such a QM effect can be taken into account [30], the calculation becomes entangled. Even for the $\bar{p}+H$ collisions at the low-

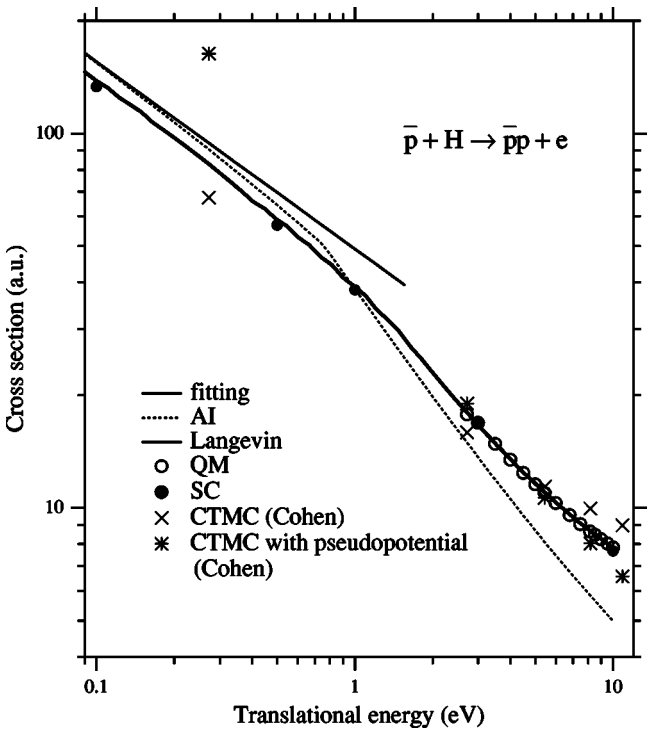

FIG. 8. $\bar{p}+H$ capture cross sections obtained by the present ("fitting" and SC) calculations, the QM calculation [18], the CTMC calculations (with and without the pseudopotentials) of Cohen [23], and the Langevin and the AI models.

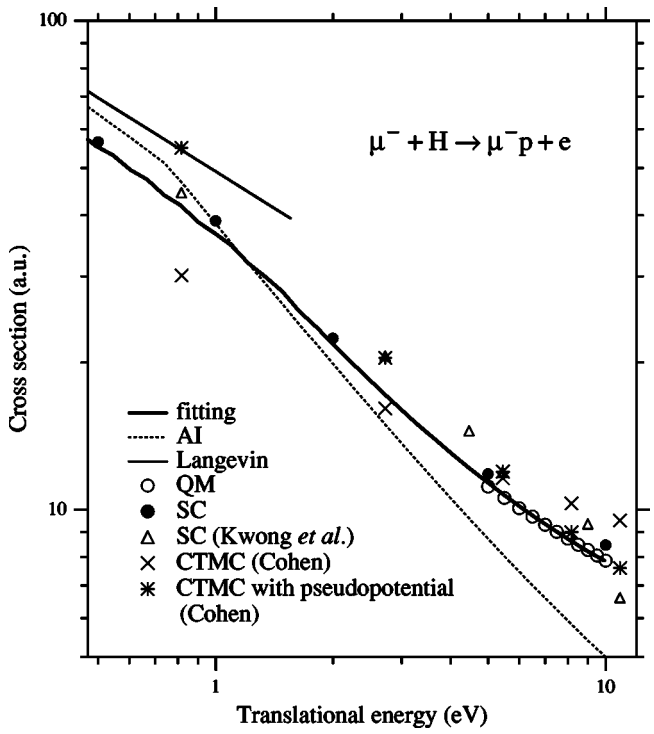

FIG. 9. $\mu^- + H$ capture cross sections obtained by the present ("fitting," QM, and SC) calculations, the SC calculation of Kwong *et al.* [25], the CTMC calculations (with and without the pseudopotentials) of Cohen [21,22], and the Langevin and the AI models.

est energy $E_t = 0.01$ eV reported here, since still a large number of partial waves ($L \lesssim 10$) contribute to the cross section, the quantum-mechanical effect may be unclear in the cross section. To avoid these complicated situations, we simply employ the classical centrifugal potential $E_t b^2/R^2$ for the calculations of the turning points in Eqs. (17) and (18). The validity of this classical treatment for the present problem is discussed in Sec. III D.

In Figs. 8 and 9, we summarize the $\bar{p}+H$ and $\mu^- + H$ capture cross sections calculated by various methods. The "fitting" cross sections obtained from Eqs. (17) and (18) agree very well with the QM results, and also with the present SC results even at low energies. For the $\mu^- + H$ collisions, the SC results of Kwong *et al.* [25] are further shown. In their SC method, the capture process is investigated by tracing a common trajectory of the relative motion, which is determined from some average potential. As mentioned in Ref. [18], such a way overestimates the capture cross section. The CTMC results of Cohen [21,22] show energy dependences different from the present results. Cohen [22,23] introduced some QM correction in the CTMC calculation by means of pseudopotentials. The results of the CTMC with pseudopotentials seem to agree with the present results at some high energies. However, the agreement becomes much worse with decreasing energies. In the AI model, the relative motion is calculated in classical mechanics with use of the adiabatic potential, and the capture cross section is assumed to be equal to the one that the closest distance becomes $R \leqslant R_{FT}$. The AI model provides the cross section much smaller than the present results at high energies and larger at very low energies. The AI cross section becomes identical to the Langevin value at $E_t \lesssim 0.1$ eV.

In Fig. 10, the "fitting" cross sections for $\bar{p}+H$ and $\mu^- + H$ (the solid lines) are compared with each other. As seen in Fig. 2, the $\bar{p}+H$ probabilities are larger than the $\mu^- + H$ ones for $R_{tp} < 1$ a.u. and are smaller for $R_{tp} > 1$ a.u. As a result, it happens that the $\bar{p}+H$ and $\mu^- + H$ cross sections agree very well with each other when $E_t \gtrsim 1$ eV. Since only the collisions with $R_{tp} < 1$ a.u. can contribute to the capture at $E_t < 1$ eV (Fig. 5), the $\bar{p}+H$ cross section is larger than the $\mu^- + H$ one at low energies ($E_t < 1$ eV). When $E_t \lesssim 0.1$ eV, the "fitting" cross sections become close to the Langevin value σ_L, and their ratios to σ_L are nearly constant. The capture cross sections at $E_t = 0.01$ eV are given by $0.88\sigma_L$ for $\bar{p}+H$ and by $0.80\sigma_L$ for $\mu^- + H$. The cross sections averaged over $E_t = 0.01 - 0.1$ eV are $0.89\sigma_L$ for $\bar{p}+H$ and $0.82\sigma_L$ for $\mu^- + H$.

D. Local complex potential

To investigate the QM effects of the relative motion at energies less than 1 eV, we further employ the LCP model. We solve the following Schrödinger equation

$$\left[-\frac{1}{2m_R}\frac{\partial^2}{\partial R^2} + \frac{L(L+1)}{2m_R R^2} + V_{real}(R) + iV_{imag}(R) - E_t \right] f(R) = 0, \tag{20}$$

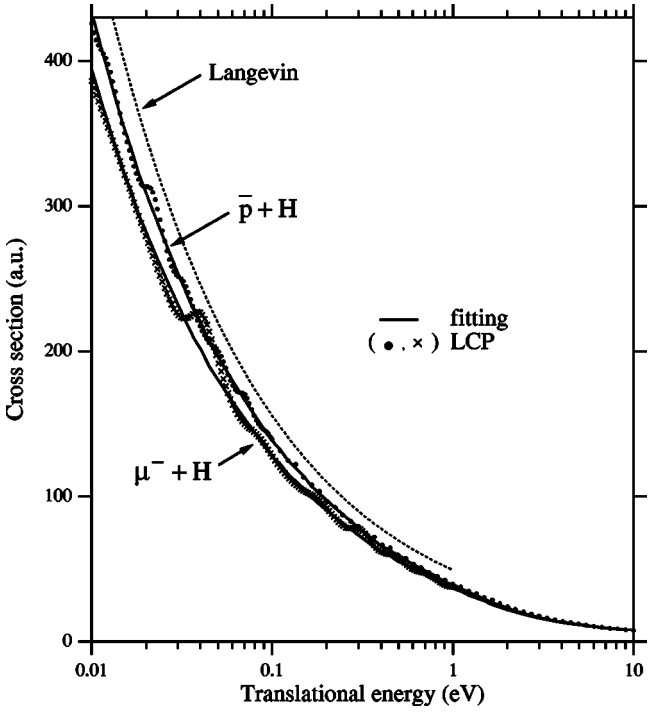

FIG. 10. $\bar{p}+\mathrm{H}$ and $\mu^-+\mathrm{H}$ capture cross sections calculated from the fitting formulas (17) and (18), and by the LCP model as a function of the translational energy E_t. The Langevin cross sections are shown for comparison.

where $V_{\mathrm{real}}(R)+iV_{\mathrm{imag}}(R)$ is the LCP. For the $X^-+\mathrm{H}$ system, Cohen *et al.* [31] considered the LCP method that is based on a diabatic-state description. Here, we construct the LCP in an empirical manner. We give the real part $V_{\mathrm{real}}(R)$ of the LCP by the adiabatic potential $V_{\mathrm{ad}}(R)$. It seems to be quite reasonable to assume that the imaginary part $V_{\mathrm{imag}}(R)$ has the form similar to the fitting formula (17) or (18). Hence, we assume $V^{X^-}_{\mathrm{imag}}(R)=-AP^{X^-}_{\mathrm{fit}}(BR)$. Adjusting the parameters A and B to fit the QM results, we have found that $A=0.027$ a.u., $B=1.08$ for $X^-=\bar{p}$; and $A=0.04$ a.u., $B=1.03$ for $X^-=\mu^-$. By solving Eq. (20), we obtain the S matrix S^L, and then the capture probability may be defined by

$$P^L_{\mathrm{LCP}}=1-|S^L|^2. \tag{21}$$

In Fig. 11, we compare the capture probabilities calculated by the LCP method with the QM results at $E_t=3$ and 5 eV. This comparison suggests that the present LCP model is reliable enough for the present purpose. Voronin and Carbonell [16] also obtained an empirical LCP for $\bar{p}+\mathrm{H}$. However, their imaginary potential produces too small capture probabilities (only about a half of the QM result) at $E_t=3$ and 5 eV. Voronin and Carbonell considered extremely-low energies ($E_t<10^{-5}$ eV) and only $L=0$ and 1. The LCP approximation would not be justified over a wide range of energy or angular momentum.

Figure 12 shows the $\bar{p}+\mathrm{H}$ and $\mu^-+\mathrm{H}$ capture probabilities obtained by the LCP method for various L. In a classical

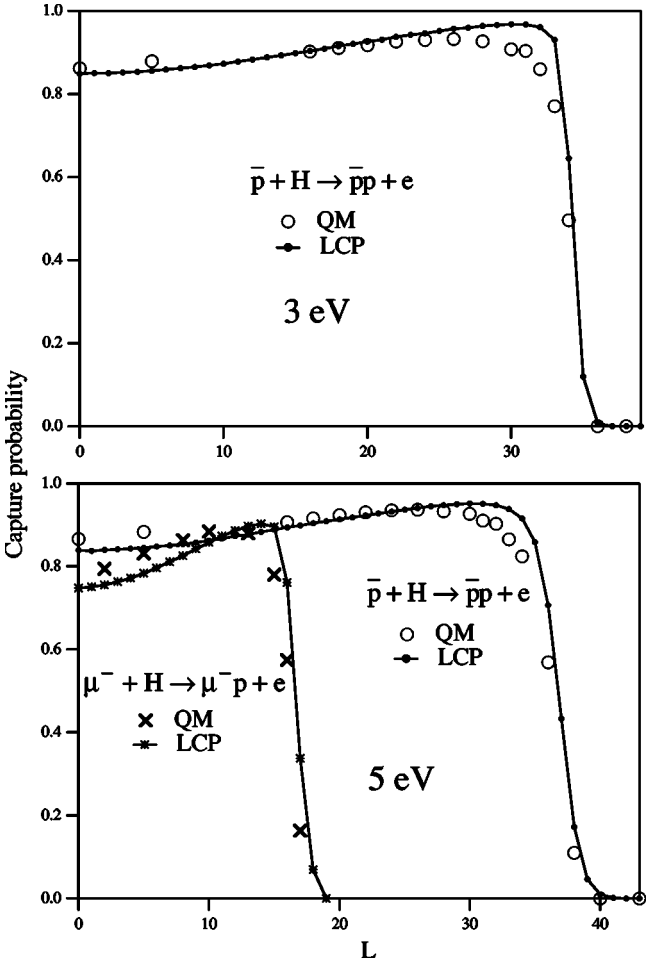

FIG. 11. $\bar{p}+\mathrm{H}$ capture probabilities obtained by the QM and the LCP calculations at $E_t=3$ and 5 eV as a function of the angular momentum L. $\mu^-+\mathrm{H}$ capture probabilities are also shown for $E_t=5$ eV.

sense, the capture can never occur if the energy is lower than the barrier height E_{max} of the effective potential $V^L_{\mathrm{eff}}(R)$. However, all the LCP probabilities are about 0.5 at $E_t\sim E_{\mathrm{max}}$, and form a slowly varying curve both below and above $E_t=E_{\mathrm{max}}$. This means that the consideration of the tunneling and the above-barrier reflection is important to describe accurately the QM feature of the relative motion.

The capture cross sections obtained by the LCP method are shown also in Fig. 10. At high energies, the LCP cross sections agree very well with the ''fitting'' results. When the energy is low, the LCP curve oscillates around the ''fitting'' result. This oscillation is caused by the potential resonances. For $\bar{p}+\mathrm{H}$, since the resonances are not so significant, it is a good approximation to neglect the oscillation around the ''fitting'' probabilities. Hence, for $\bar{p}+\mathrm{H}$ at the energies reported here, we may conclude that the inclusion of all the QM effects results in only a very small deviation from the pure classical description of the relative motion. The resonances in the LCP calculation are more pronounced for $\mu^-+\mathrm{H}$, and accordingly the μ^- cross section becomes larger than the $\bar{p}$ one at $E_t\sim 0.04$ eV. Nevertheless, we can expect

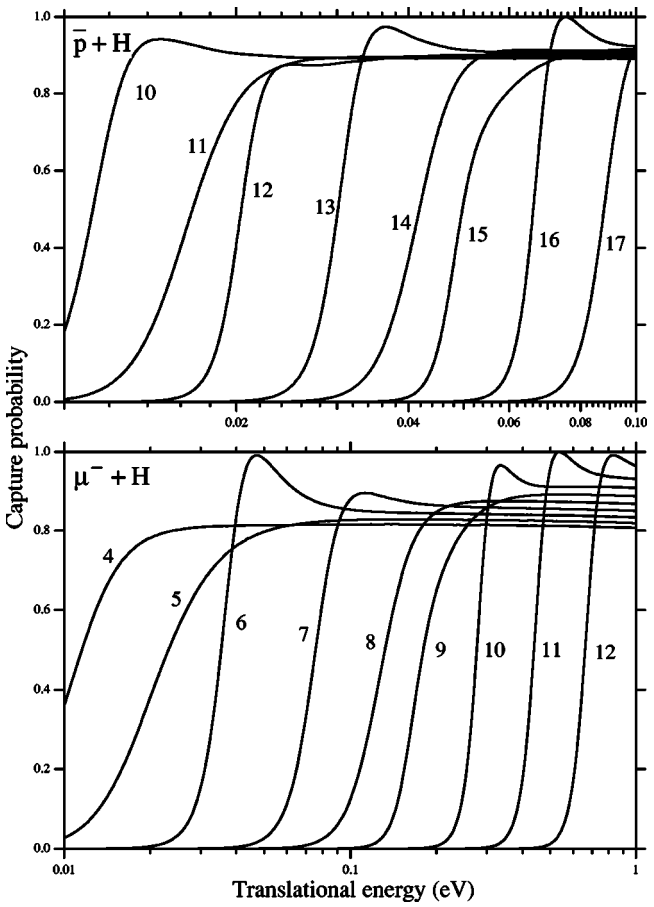

FIG. 12. Capture probabilities obtained by the LCP calculation as a function of the translational energy E_t. The partial waves $L=10$–17 are shown in the energy range $E_t=0.01$–0.1 eV for $\bar{p}+\mathrm{H}$. The partial waves $L=4$–12 are shown in the energy range $E_t=0.01$–1 eV for $\mu^-+\mathrm{H}$.

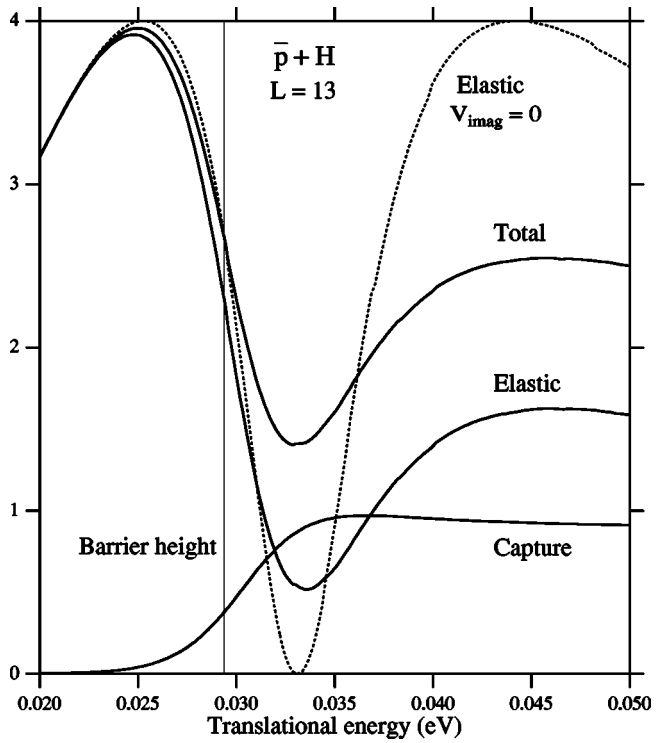

FIG. 13. $\bar{p}+\mathrm{H}$ capture probabilities (P^L_{LCP}), elastic (Q^L_{el}) and total (Q^L_{tot}) quantities (see text) obtained by the LCP calculation as a function of the translational energy E_t for $L=13$. The results of the elastic collisions obtained by assuming $V_{\mathrm{imag}}(R)=0$ are also shown. A vertical thin line indicates the barrier height of the effective potential $V^{L=13}_{\mathrm{eff}}(R)$.

that the pure classical description of the relative motion is still useful to see the global feature of the capture cross sections even for $\mu^-+\mathrm{H}$.

In the present SC method, the calculation has been carried out by using Eq. (14) with discrete L. The present study suggests that the pure classical description is better for the relative motion after all. Hence, the classical centrifugal potential $E_t b^2/R^2$ with continuous b should be rather used in Eq. (14) to obtain a more reliable capture cross section. However, the energies shown in Figs. 8 and 9 are sufficiently high so that we can neglect the discreteness of L in the calculation of the capture cross section.

E. Resonances

From Fig. 12, we see that the resonances come from the partial waves $L=10$, 12, 13, and 16 for $\bar{p}+\mathrm{H}$ and from $L=6$, 7, 10, 11, and 12 for $\mu^-+\mathrm{H}$. To see more details of the resonance, Fig. 13 shows some quantities which characterize the collision in $\bar{p}+\mathrm{H}$ for $L=13$. The elastic cross section for each L is proportional to $Q^L_{\mathrm{el}}=|1-S^L|^2$, and the total cross section for each L is proportional to $Q^L_{\mathrm{tot}}=P^L_{\mathrm{LCP}}+Q^L_{\mathrm{el}}$. In Fig. 13, we also plot the elastic quantity Q^L_{el} obtained by setting $V_{\mathrm{imag}}=0$. In the elastic collision with $V_{\mathrm{imag}}=0$, the resonance appears as a window since the nonresonant (background) part has the maximum contribution at the related energies. When V_{imag} is very strong, the resonance profile is largely affected by the presence of the imaginary potential. Here, we simply define the resonance position E_{res} by the minimum (or maximum) position of the elastic resonance window (or peak) with $V_{\mathrm{imag}}=0$. As shown in Fig. 13, the resonance position E_{res} is larger than the barrier height E_{max} of $V^L_{\mathrm{eff}}(R)$. Therefore, this is an above-barrier (AB) resonance.

In Table I, we summarize some properties of the resonances observed in Fig. 12. A quasi-bound (QB) resonance that occurs below the barrier height is only seen for $L=12$ in $\bar{p}+\mathrm{H}$ and for $L=6$ in $\mu^-+\mathrm{H}$. Furthermore, the $L=12$ resonance in $\bar{p}+\mathrm{H}$ is not so remarkable. Therefore, except for the most prominent resonance of $L=6$ in $\mu^-+\mathrm{H}$, we can see that the AB resonance plays a more important role in the capture process.

Figure 10 shows that the resonance effect on the capture cross section is not very significant, and the global behavior of the cross section at low energies is mostly explained by the Langevin model. Prominent resonance structures due to QB states were found previously in several theoretical studies of ion-atom reactive collisions, such as electron transfer [32–35] and radiative association [36,37]. Also in the present

TABLE I. Resonance features of the elastic collisions by the adiabatic potential (with $V_{\mathrm{imag}}=0$) in the energy ranges shown in Fig. 12.

L	E_{res}	E_{max}	Type	Shape
$\bar{p}+\mathrm{H}$				
10	0.0140	0.0107	AB	Window
12	0.0208	0.0215	QB	Window
13	0.0329	0.0294	AB	Window
16	0.0679	0.0665	AB	Window
$\mu^-+\mathrm{H}$				
6	0.0378	0.0383	QB	Peak
7	0.0769	0.0688	AB	Peak
10	0.299	0.288	AB	Window
11	0.480	0.435	AB	Window
12	0.707	0.647	AB	Window

case, the QB resonances might become much significant if the reactivity were suppressed. To confirm this, we have reduced the strength of the imaginary potential artificially, and have carried out the LCP calculations for $\bar{p}+\mathrm{H}$. Figure 14 shows the calculated capture probabilities for $L=15$ with use of the imaginary parts $V_{\mathrm{imag}}(R)=cV^{\bar{p}}_{\mathrm{imag}}(R)$, where $c=1$, 0.5, 0.3, and 0.1. In the original case ($c=1$), we have no resonance structure. When $c\leqslant 0.5$, however, the QB resonance becomes more prominent with decreasing the strength of the imaginary potential. A similar finding for the dependence of the imaginary potential was also obtained in associative detachment of $\mathrm{H}^-+\mathrm{H}$ [38]. As a matter of course, the reaction cross section becomes much smaller than the Langevin value when the strength of the imaginary potential is very weak. Probably, it is generally true that the effect of the resonances is less significant in the ion-molecule reaction when the reaction cross section is very close to the Langevin value over a wide energy range.

IV. SUMMARY AND CONCLUSION

We have carried out the QM calculations for $\mu^-+\mathrm{H}$ and $K^-+\mathrm{H}$ at $5\leqslant E_{\mathrm{t}}\leqslant 10$ eV, and the SC calculations for $\mu^-+\mathrm{H}$ and $\bar{p}+\mathrm{H}$ at $0.1\leqslant E_{\mathrm{t}}\leqslant 10$ eV. We have found that the empirical law is satisfied for the relation between the capture probability P^L and the classical turning point R_{tp} of the relative motion. The same fitting formula of P^L vs R_{tp} can be used in $K^-+\mathrm{H}$ and in $\bar{p}+\mathrm{H}$. The fitting formula becomes slightly different in $\mu^-+\mathrm{H}$ because of the large mass difference.

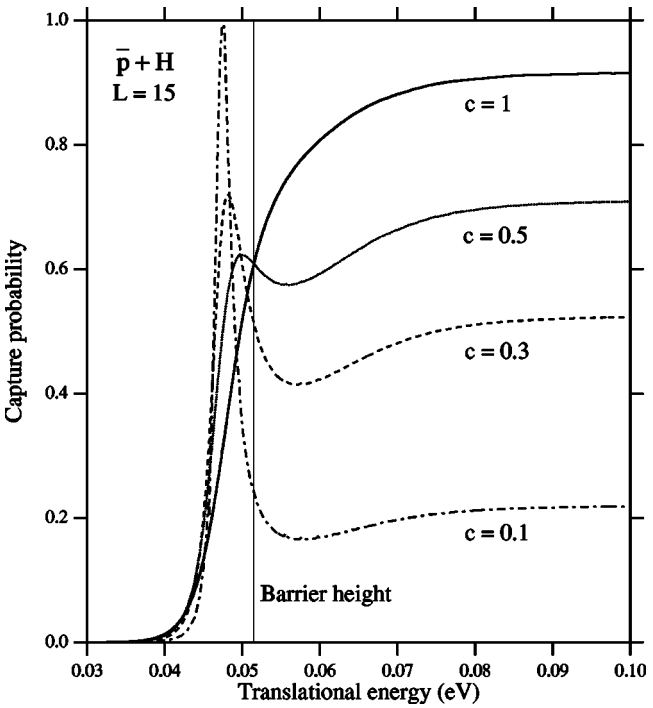

FIG. 14. $\bar{p}+\mathrm{H}$ capture probabilities obtained by the LCP calculation as a function of the translational energy E_{t} for $L=15$. The strengths of the imaginary potential are taken to be $V_{\mathrm{imag}}(R)=cV^{\bar{p}}_{\mathrm{imag}}(R)$, where $c=1$, 0.5, 0.3, and 0.1. A vertical thin line indicates the barrier height of the effective potential $V^{L=15}_{\mathrm{eff}}(R)$.

The capture cross sections at $E_{\mathrm{t}}\gtrsim 1$ eV are almost the same for the three systems of $\mu^-+\mathrm{H}$, $K^-+\mathrm{H}$, and $\bar{p}+\mathrm{H}$. When $E_{\mathrm{t}}<1$ eV, the μ^- cross section becomes smaller than the $\bar{p}$ one.

The capture processes at very low energies have been studied by using the LCP model. When $E_{\mathrm{t}}<0.1$ eV, the capture cross section is close and nearly proportional to the Langevin value. Some interesting resonance structures are seen in the capture cross section. However, the resonance effect is not exceedingly drastic in the present case. Since the LCP approximation is a quite simplified model, an accurate QM description will be needed to discuss the details of these resonances. The extension of the present time-dependent QM calculation to this low-energy region is very interesting.

ACKNOWLEDGMENT

This research was partially supported by the Grant-in-Aid for Scientific Research from the Ministry of Education, Science, Sports, and Culture, Japan.

[1] A. Adamo *et al.*, Phys. Rev. A **47**, 4517 (1993).
[2] M. Agnello *et al.*, Phys. Rev. Lett. **74**, 371 (1995).
[3] H. Knudsen, H.U. Mikkelsen, K. Paludan, K. Kirsebom, S.P. Møller, J.E. Uggerhøj, J. Slevin, M. Charlton, and E. Morenzoni, Phys. Rev. Lett. **74**, 4627 (1995).
[4] G. Schiwietz, U. Wille, R. Díez Muiño, P.D. Fainstein, and P.L. Grande, J. Phys. B **29**, 307 (1996), and references therein.
[5] E. Widmann, I. Sugai, T. Yamazaki, R.S. Hayano, M. Iwasaki, S.N. Nakamura, H. Tamura, T.M. Ito, A. Kawachi, N. Nishida, W. Higemoto, Y. Ito, N. Morita, F.J. Hartmann, H. Daniel, T. von Egidy, W. Schmid, J. Hoffmann, and J. Eades, Phys. Rev. A **53**, 3129 (1996).

[6] J. Eades and F.J. Hartmann, Rev. Mod. Phys. **71**, 373 (1999).
[7] M.H. Holzscheiter and M. Charlton, Rep. Prog. Phys. **62**, 1 (1999).
[8] A.S. Wightman, Phys. Rev. **77**, 521 (1950).
[9] G.T. Condo, Phys. Lett. **9**, 65 (1964).
[10] J.T. Russell, Phys. Rev. A **1**, 721 (1970).
[11] T. Yamazaki, M. Aoki, M. Iwasaki, R.S. Hayano, T. Ishikawa, H. Outa, E. Takada, H. Tamura, and A. Sakaguchi, Phys. Rev. Lett. **63**, 1590 (1989).
[12] M. Iwasaki, S.N. Nakamura, K. Shigaki, Y. Shimizu, H. Tamura, T. Ishikawa, R.S. Hayano, E. Takada, E. Widmann, H. Outa, M. Aoki, P. Kitching, and T. Yamazaki, Phys. Rev. Lett. **67**, 1246 (1991).
[13] S.N. Nakamura, M. Iwasaki, H. Outa, R.S. Hayano, Y. Watanabe, T. Nagae, T. Yamazaki, H. Tada, T. Numao, Y. Kuno, and R. Kadono, Phys. Rev. A **45**, 6202 (1992).
[14] N. Morita, M. Kumakura, T. Yamazaki, E. Widmann, H. Masuda, I. Sugai, R.S. Hayano, F.E. Maas, H.A. Torii, F.J. Hartmann, H. Daniel, T. von Egidy, B. Ketzer, W. Müller, W. Schmid, D. Horváth, and J. Eade, Phys. Rev. Lett. **72**, 1180 (1994).
[15] H.A. Torii, R.S. Hayano, M. Hori, T. Ishikawa, N. Morita, M. Kumakura, I. Sugai, T. Yamazaki, B. Ketzer, F.J. Hartmann, T. von Egidy, R. Pohl, C. Maierl, D. Horváth, J. Eades, and E. Widmann, Phys. Rev. A **59**, 223 (1999).
[16] A.Y. Voronin and J. Carbonell, Phys. Rev. A **57**, 4335 (1998).
[17] J.D. Garcia, B.H. Kwong, and J.S. Cohen, Phys. Rev. A **35**, 4068 (1987).
[18] K. Sakimoto, Phys. Rev. A **65**, 012706 (2002).
[19] K. Sakimoto, J. Phys. B **35**, 997 (2002).
[20] K. Sakimoto, J. Phys. B **33**, 3149 (2000).
[21] J.S. Cohen, Phys. Rev. A **27**, 167 (1983).
[22] J.S. Cohen, Phys. Rev. A **56**, 3583 (1997).
[23] J.S. Cohen, J. Phys. B **31**, L833 (1998).
[24] D.R. Schultz, P.S. Krstić, C.O. Reinhold, and J.C. Wells, Phys. Rev. Lett. **76**, 2882 (1996).
[25] N.H. Kwong, J.D. Garcia, and J.S. Cohen, J. Phys. B **22**, L633 (1989).
[26] D.L. Morgan, Jr., and V.W. Hughes, Phys. Rev. A **7**, 1811 (1973).
[27] G. Gioumousis and D.P. Stevenson, J. Chem. Phys. **29**, 294 (1958).
[28] M.E. Rose, *Elementary Theory of Angular Momentum* (Wiley, New York, 1957).
[29] K. Sakimoto, J. Phys. B **34**, 1769 (2001).
[30] N. Fröman, in *Semiclassical Methods in Molecular Scattering and Spectroscopy*, Vol. 53 of *NATO Advanced Study Institute, Series C: Mathematical and Physical Sciences*, edited by M.S. Child (Reidel, Dordrecht, 1980), pp. 1–44.
[31] J.S. Cohen R.L. Martin, and W.R. Wadt, Phys. Rev. A **24**, 33 (1981).
[32] J.P. Davis and W.R. Thorson, Can. J. Phys. **56**, 996 (1978).
[33] B.W. West, N.F. Lane, and J.S. Cohen, Phys. Rev. A **26**, 3164 (1982).
[34] N. Shimakura and M. Kimura, Phys. Rev. A **44**, 1659 (1991).
[35] B.D. Esry, H.R. Sadeghpour, E. Wells, and I. Ben-Itzhak, J. Phys. B **33**, 5329 (2000).
[36] H. Abgrall, A. Giusti-Suzor, and E. Roueff, Astrophys. J. Lett. **207**, L69 (1976).
[37] M.M. Graff, J.T. Moseley, and E. Roueff, Astrophys. J. **269**, 796 (1983).
[38] K. Sakimoto, Chem. Phys. Lett. **164**, 294 (1989).